The Knee 26 (2019) 1220–1233

Contents lists available at ScienceDirect

The Knee

Mechanical characterization of the ligaments in subject-specific models of the patellofemoral joint using in vivo laxity tests

Mohammad Akbar [a], Farzam Farahmand [a,b,*], Navid Arjmand [a]

[a] Mechanical Engineering Department, Sharif University of Technology, Tehran, Iran
[b] RCBTR, Tehran University of Medical Sciences, Tehran, Iran

ARTICLE INFO

Article history:
Received 20 February 2018
Received in revised form 22 June 2018
Accepted 2 October 2018

Keywords:
Biplane fluoroscopy
Laxity test
MPFL
LPFL
Patellar shift
Patellar tilt

ABSTRACT

Background: The purpose of this study was to propose a methodology for mechanical characterization of the ligaments in subject-specific models of the patellofemoral joint (PFJ) of living individuals.
Method: PFJ laxity tests were performed on a healthy volunteer using a specially designed loading apparatus under biplane fluoroscopy. A three-dimensional (3D) parametric model of the PFJ was developed in the framework of the rigid body spring model using the geometrical data acquired from the subject's computed tomography and magnetic resonance images. The stiffness and pre-strains of the medial and lateral PFJ ligaments were characterized using a two-step optimization procedure which minimized the deviation between the model predictions and the calibration test results. Sensitivity analyses were performed to investigate the effect of mechanical properties of the non-characterized model components on the characterization procedure and its results.
Results: The overall findings indicate that the proposed methodology is applicable and can improve the model predictions effectively. For the subject under study, ligament characterization reduced the root mean square of the deviations between the patellar shift and tilt predicted by the model and obtained experimentally for the validation laxity test (from 6.2 mm to 0.5 mm, and from 8.4° to 1.5°, respectively) and passive knee flexion test (from 1.4 mm to 0.3 mm, and from 2.3° to 1.3°, respectively). The non-characterized mechanical properties were found to have a minimal effect on the characterization procedure and its results.
Conclusion: The proposed methodology can help in developing truly patient-specific models of the PFJ, to be used for personalized preplanning of the clinical interventions.

1. Introduction

Subject-specific joint models (SSJMs) have been extensively used in recent years to provide a more detailed insight into the biomechanics of human joints [1–10]. Another attractive application of these models, however, is simulation of a joint disorder and the prospective surgical/conservative interventions for a specific patient [11–13]. With such capability, the SSJMs could emerge as useful clinical tools to help with understanding the etiology of a disorder more precisely and preplanning more effective personalized treatments.

* Corresponding author at: Biomechanics Section, Mechanical Engineering Department, Sharif University of Technology, Azadi Avenue, Tehran, Iran.
E-mail address: farahmand@sharif.edu. (F. Farahmand).

https://doi.org/10.1016/j.knee.2018.10.001
0968-0160/

There are two main types of information required to build an SSJM: (1) the geometry of the joint components, and (2) the mechanical properties of the joint structures. The existing SSJMs of living individuals [2,6,7,9] are geometrically subject specific only, i.e. the articulating surfaces, muscle action lines, and ligament attachment points are obtained using in vivo computed tomography (CT) and/or magnetic resonance (MR) imaging of the subject under study. For the mechanical properties of the joint structures, e.g., the stiffness and pre-tension of the ligaments, however, they use some average in vitro data from the literature. It has been reported that neglecting the inter-individual variability for the mechanical properties of the ligamentous tissues can greatly affect the efficacy of the SSJMs in predicting the results of surgical interventions [14].

The patellofemoral joint (PFJ), is a prominent example of a human joint, in which the passive soft tissues play an important role in the joint stability behavior. In vitro biomechanical studies have shown that while the patellar stability within the femoral groove after 20° knee flexion is mainly provided by the restraining effects of the articulating surfaces [15], it is contributed largely by the medial patellofemoral ligament (MPFL) and the lateral patellofemoral ligament (LPFL) near full extension [16,17]. This is particularly the case when the quadriceps tension is minimal, e.g., during the terminal swing phase of the gait cycle, at which the patellar dislocation happens most frequently [18]. Clinical literature indicates that the PFJ problems, in the forms of subluxation, dislocation and patellofemoral pain syndrome are associated with patellar insufficient mechanical stability within the femoral groove, in the early knee flexion range [19,20]. Moreover, it has been reported that MPFL deficiency is a major cause of patellar instability disorders near full extension and its reconstruction improves the patellar tracking within the groove [21–23].

In spite of the critical role of the PFJ ligaments in the joint stability behavior, shown in biomechanical and clinical investigations, neither of the previous PFJ models of living individuals [4,7,8,10,24] has provided a solution for representing the real subject-specific mechanical responses of the ligaments. The purpose of this study, hence, was to propose a methodology for developing geometrically and mechanically SSJMs of the PFJ of living individuals, based on the mechanical characterization of the ligaments. A parametric PFJ model was developed which included a detailed representation of the articulating surfaces, cartilaginous layers, quadriceps muscles, and ligamentous tissues, with the geometries of the model components extracted from CT and MR images. The mechanical properties of the MPFL and LPFL were then found using a model-based inverse characterization approach which incorporated the results of in vivo laxity tests performed under biplane fluoroscopy. The joint tracking data needed for simulation, as well as validation of the model predictions, were also obtained using biplane fluoroscopy imaging. The model was then used in a number of simulation studies to assess the effect of mechanical characterization on its predictions for the patellar tilt and shift, in comparison with the experimental results. It was hypothesized that characterization of the mechanical properties of the ligaments in a geometrically subject-specific PFJ model could improve the model's predictions for the joint stability behavior, as required for surgical preplanning applications.

2. Method

The SSJM of the PFJ was constructed in three steps: (1) The geometrical, tracking and laxity test data was extracted from the PFJ of a healthy volunteer using CT, MR imaging and biplane fluoroscopy. (2) A geometrical SSJM was developed, in which the MPFL and LPFL were parametrically modeled. (3) The mechanical properties of the PFJ ligaments were characterized using a model-based inverse characterization approach which minimized the root mean square error between the model's predictions and the experimental results of the laxity tests. The SSJM was then utilized in a number of simulation studies to investigate the effect of the ligament characterization on the model's predictions. Also, sensitivity analyses were performed to assess the fidelity of the proposed methodology and the significance of the ligament characterization.

2.1. Experiments

A healthy male volunteer (180 cm, 84 kg, 30 years), with no history of PFJ disorder, participated in this study, after obtaining the institution's ethical committee's approval and informed consent. The geometrical data of the femoral and patellar articular surfaces were acquired using CT imaging (BrightSpeed, GE, USA) with a resolution of $0.707 \times 0.707 \times 1$ mm, while the subject was lying supine with fully extended legs and relaxed quadriceps. Also, the geometries of the cartilage and the muscular and ligamentous tissues were obtained using MR imaging (Trio Tim, Siemens, Germany) with a resolution of $0.5 \times 0.5 \times 0.5$ mm, in the same posture. The latter data included the attachment sites of the quadriceps muscles, the MPFL, the LPFL and the patellar tendon into the bones, which were identified using the guidelines of the anatomical atlases and the literature [25–29].

At first, a passive knee flexion test was performed in which the subject's knee was flexed from full extension to 45° flexion, while he was lying prone under a biplane fluoroscopy system (Axiom Artis BA, Siemens) with a resolution of 1024×1024 and frontal and lateral detector sizes of 38×30 cm and 25×25 cm, respectively. During this test, the subject was asked to relax his muscles and an assistant held the middle of the shank and moved it slowly upwards. The positions of the femur, patella and tibia were recorded during the test by the two detectors, after calibration [30].

In the next step, the PFJ laxity tests were conducted using a specially designed patellar loading apparatus (Figure 1) under the same biplane fluoroscopy system. The three-dimensional (3D) position and orientation of the loading apparatus with respect to the patella could be fixed as desired using a number of adjusting mechanisms. A loading lever, controlled manually, was used to move a loading tip (Figure 1) that applied a perturbing force to the patella along the adjusted direction. The magnitude of the perturbing force was recorded using a high-accuracy (force error: ± 0.04 N; torque error: ± 0.05 Nmm) six-axis force transducer (Nano 25-E, ATI Industrial Automation, Apex, USA) embedded inside the apparatus. Also, the 3D direction of the force (loading tip), as well as the bones' motions, were recorded using the biplane fluoroscopy system.

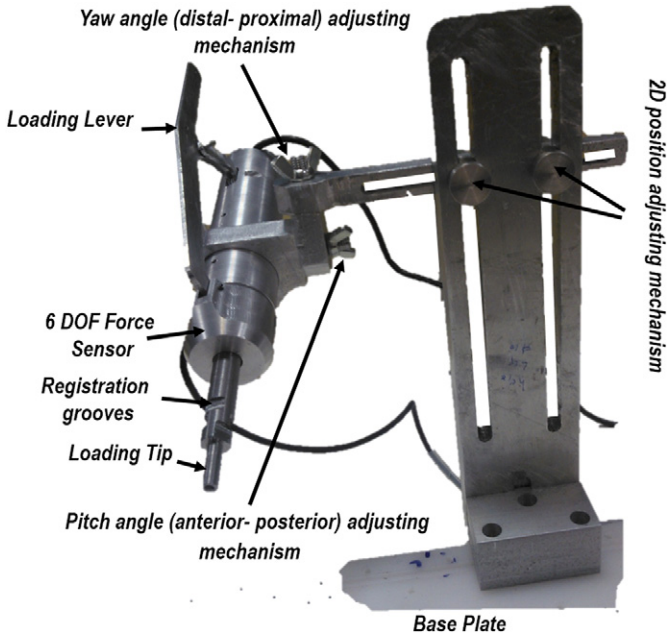

Figure 1. Specially designed patellar loading apparatus used for three-dimensional patellofemoral joint laxity tests. Adjusting the mechanisms enables fixing the apparatus at the desired position and orientation with respect to the patella. Loading lever moves the loading tip to apply a perturbing force to the patella which is measured using the six-axis force transducer.

The laxity tests were performed in five test configurations, specified by the perturbing force direction and the knee flexion angle (Table 1). During each test, after adjusting the position and orientation of the loading apparatus, the operator pushed the loading lever to apply an increasing perturbing force to the patellar lateral or medial edge, towards medial or lateral, respectively, while the subject was lying supine, with the quadriceps relaxed and the knee kept fixed between 0° and 15° by means of a wedge (Figure 2). The test was terminated when a maximum force of 50 N or a maximum displacement of 20 mm at the loading tip was reached. To ensure repeatability of the experiments, each test was repeated at least three times. From the five test configurations,

Table 1
Configurations of the patellofemoral joint laxity tests.

Test no.	Test point	Knee flexion angle	Patellar perturbing force			
			Yaw angle (Distal–proximal)	Pitch angle (Medial–lateral)	Application point	Magnitude (N)
1	1.1	$\approx 5^{\circ}$	$\approx 0^{\circ}$	$\approx 30^{\circ}$	Patellar medial edge	0
	1.2					9.2
	1.3					17.3
	1.4					24.9
	1.5					32.4
2	2.1	$\approx 15^{\circ}$	$\approx 0^{\circ}$	$\approx 30^{\circ}$	Patellar medial edge	0
	2.2					14.2
	2.3					20.1
	2.4					28.4
	2.5					39.3
3	3.1	$\approx 10^{\circ}$	$\approx 180^{\circ}$	$\approx -30^{\circ}$	Patellar lateral edge	0
	3.2					11.2
	3.3					24.9
	3.4					36.5
	3.5					48.0
4	4.1	$\approx 0^{\circ}$	$\approx 180^{\circ}$	$\approx -30^{\circ}$	Patellar lateral edge	0
	4.2					8.1
	4.3					19.0
	4.4					25.8
	4.5					32.3
5	5.1	$\approx 10^{\circ}$	$\approx 30^{\circ}$	$\approx 15^{\circ}$	Patellar medial edge	0
	5.2					5.9
	5.3					17.1
	5.4					23.0
	5.5					33.7

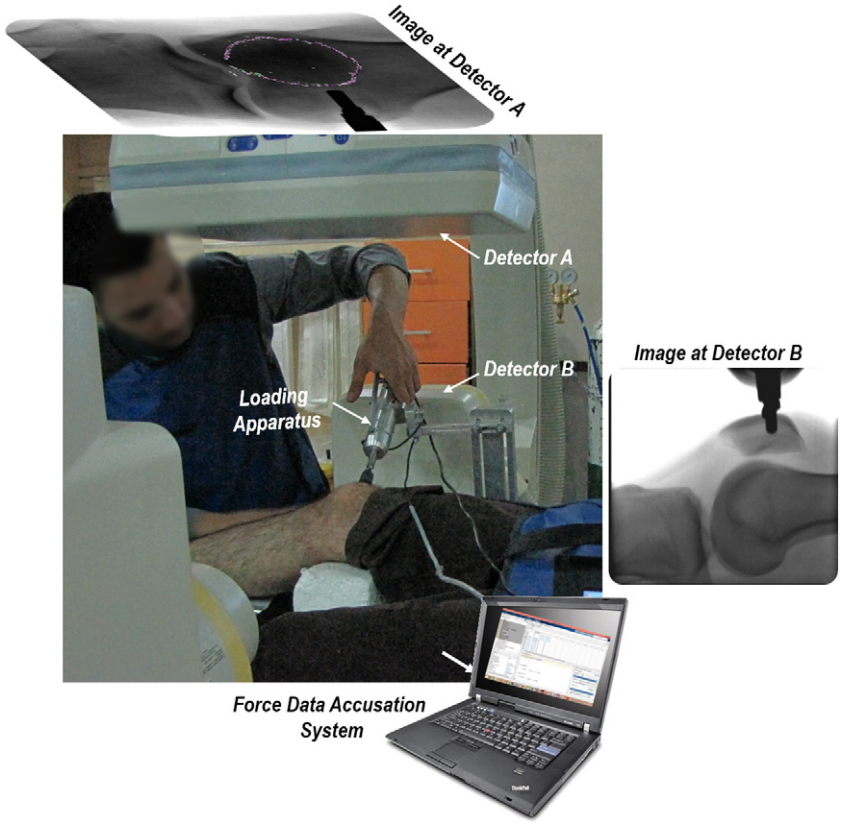

Figure 2. The setup and procedure of the three-dimensional (3D) laxity tests. With the knee flexion fixed, the patella was pushed towards medial or lateral, using the patellar loading apparatus. The 3D tracking of the bones and the loading tip (direction of the perturbing force) were recorded using biplane fluoroscopy (detectors A and B). The magnitude of the perturbing force was acquired using the force transducer embedded inside the loading apparatus.

the first four were considered as the calibration tests and the other one as the validation test. Five test points (at 0, 25, 50, 75 and 100% of the maximum perturbing force) were extracted from the results of each test for analysis (Table 1).

The 3D orientation of the loading tip, as well as the 3D tracking data of the patella, femur and tibia in the fluoroscopy coordinate system, were found at each test point using a two dimensional (2D)–3D registration algorithm [31–33] (Figure 3). Registration procedure was performed manually using an in-house code (MATLAB 7.10.0, Mathworks Inc., Natick, MA, USA). The 3D models of the bones and the loading tip, constructed from CT images, were translated and rotated in 3D such that the contours of their digitally reconstructed radiographs (DRRs) matched those of the fluoroscopy images (Figure 3(a–c)). The precision of this registration method, tested on human cadaver bones, revealed orientation and translation errors in the ranges of $\pm 0.55^{\circ}$ and ± 0.35 mm, respectively [34].

Finally, all the geometrical and tracking data were registered into the biomechanical coordinate systems of the femur and patella, defined based on the anatomical landmarks of the bones (Figure 4). The registration of the MR coordinate system into the CT coordinate system was performed using a rigid 3D–3D registration method, which matched the bones' anatomical landmarks with an accuracy of ± 0.20 mm [2]. For the tracking data, a series of matrix transformations were applied to transfer them from the fluoroscopy coordinate system into the CT coordinate system, and then the bones' biomechanical coordinate systems. The tracking data of the femur, the tibial tubercle, and the loading tip were transferred into the femoral coordinate system, and that of the patella to the patellar coordinate system. The patellar translations and rotations with respect to the femur were described using the position and orientation of the patellar coordinate system relative to the femoral coordinate system. The patellar rotations around X_F, Y_p, and Z_p axes were considered as flexion, tilt, and rotation, and its translations along X_F, Y_F, and Z_F axes as shift, distal–proximal and anterior–posterior translation, respectively (Figure 4).

2.2. PFJ modeling

A 3D parametric model of the PFJ was developed using the geometrical data of the subject, acquired from the experiments. The model included the femoral and patellar articulating surfaces (including their cartilage layers), the six components of the quadriceps muscles (rectus femoris, vastus intermedius, vastus medialis longus, vastus medialis obliquus, vastus lateralis longus, and vastus lateralis obliquus), the MPFL and LPFL, and the patellar tendon (Figure 5). Details of the model are described in the authors'

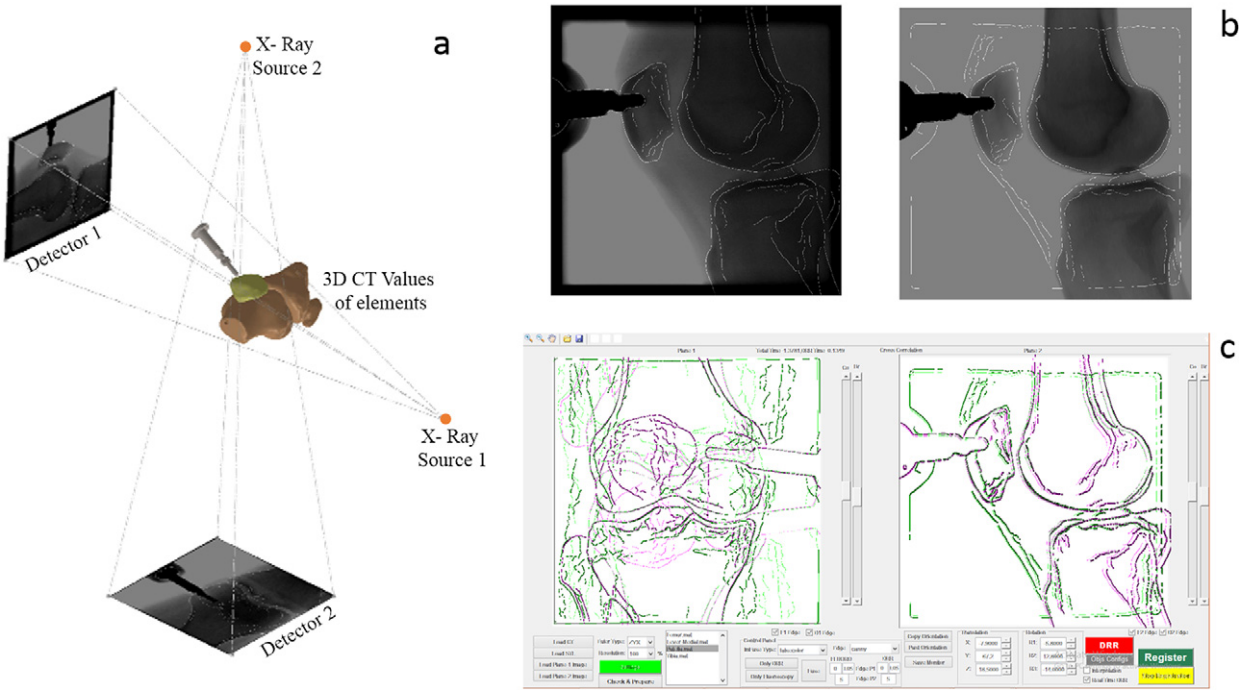

Figure 3. Schematics of the registration procedure used to find the three-dimensional (3D) tracking of the bones and the loading tip during laxity tests from biplane fluoroscopic images. (a) Generating the digitally reconstructed radiographs (DRRs) from the 3D models of the bones and the loading tip. (b) Extracting the contours from fluoroscopic (left) and DRR (right) images. (c) Registration of the counters in frontal (left) and sagittal (right) planes.

previous publication [2]. In brief, the patella and femur were modeled as rigid bodies, covered with discretized columns of deformable cartilage, in the framework of a rigid body spring model [35,36]. Each cartilage column was represented using a Kelvin viscoelastic model with mechanical constants from the literature [2]. The MPFL and LPFL were modeled as a three-bundle nonlinear

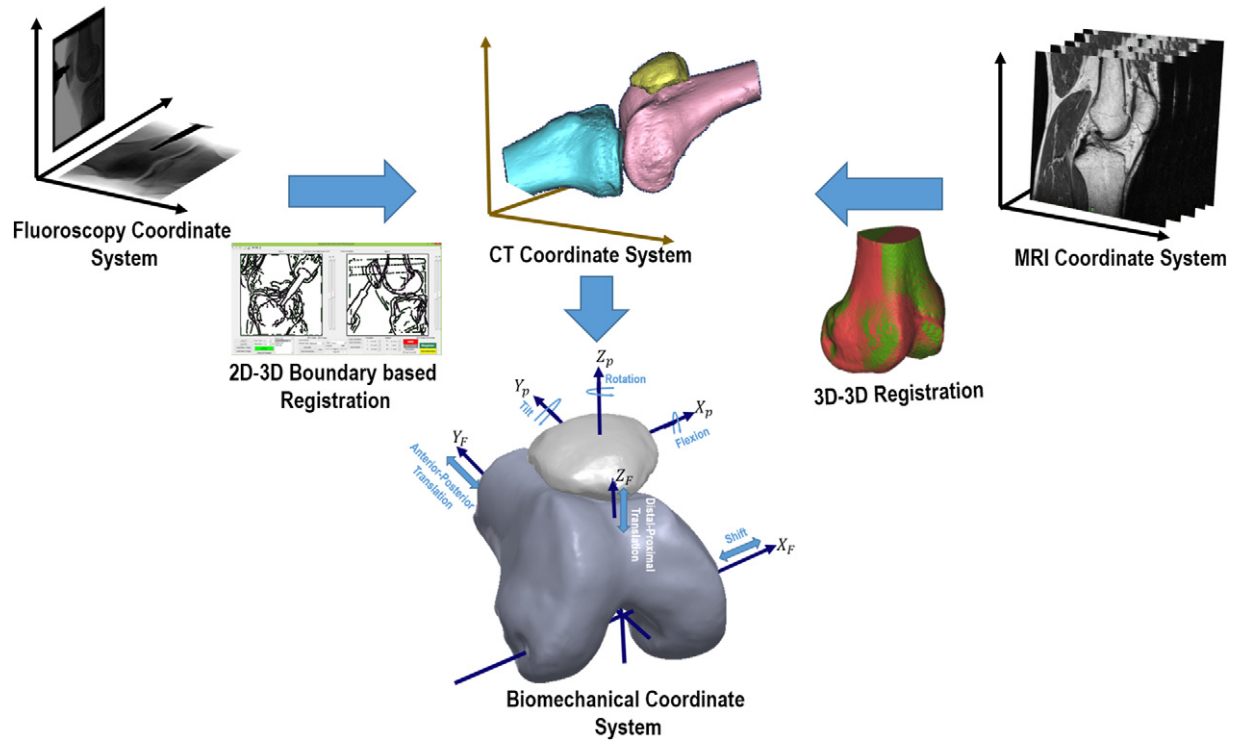

Figure 4. Schematics of the registration procedure used to transfer all geometrical and kinematic data into the biomechanical coordinate systems of the femur and patella.

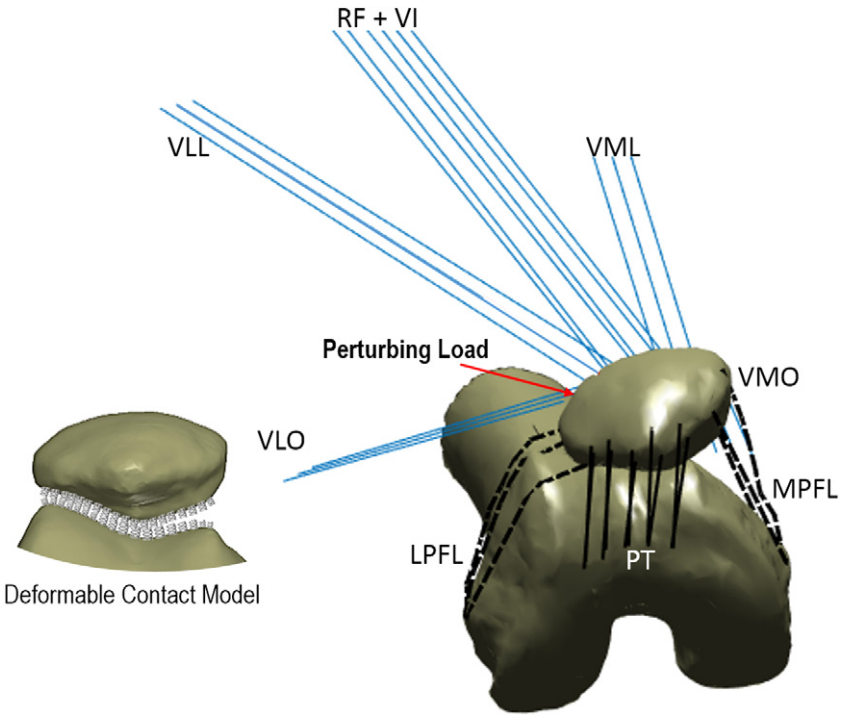

Figure 5. The patellofemoral joint model, including the femoral and patellar articulating surfaces and their articular cartilage layers, the medial patellofemoral ligament (MPFL) and the lateral patellofemoral ligament (LPFL), the patellar tendon (PT) and the quadriceps muscle components, i.e. rectus femoris (RF), vastus intermedius (VI), vastus medialis longus (VML), vastus medialis obliquus (VMO), vastus lateralis longus (VLL) and vastus lateralis obliquus (VLO). The perturbing force applied to the patella during laxity tests is also shown in the figure.

tensile spring each, and the patellar tendon as a 10-bundle linear tensile spring, to consider their broad attachment sites into the patella and femur.

In order to account for the wrapping of the MPFL and LPFL over the femoral condyles during the laxity tests (Figure 1), they were modeled in more detail, in comparison with our previous work [2]. Each ligament bundle was segmented using eight virtual nodes. For each of the nine segments of each of the six bundles of the MPFL and LPFL (in total), a nonlinear elastic behavior was considered using a piecewise force–strain relationship, as in Eq. (1) [7,37–39]:

$$f_{ij}(N)=\begin{cases}0 & \varepsilon_{ij}<0\\ \frac{1}{4}k_{ij}\cdot\varepsilon_{ij}^{\,2}/\varepsilon_1 & 0\le\varepsilon_{ij}\le 2\varepsilon_1\\ k_{ij}\left(\varepsilon_{ij}-\varepsilon_1\right) & \varepsilon_{ij}>2\varepsilon_1\end{cases}\quad i=1,2,\ldots,9 \text{ and } j=1,2,\ldots,6 \tag{1}$$

where $f_{ij}(N)$, k_{ij} (N), and ε_{ij} represent the force, strain stiffness and strain of the *ith* segment of the *jth* bundle, respectively. Also, ε_1 is half of the strain limit, set as 0.03 [38], at which the initial nonlinear behavior of the ligament in the toe region of its force–stain curve turns into a linear behavior [40]. The segmental stiffness was the same for all segments of each ligament bundle as in Eq. (2):

$$k_{ij}=9l_j^r\cdot k_j \tag{2}$$

where k_j (N/mm) and l_j^r(mm) are the elongation stiffness and the reference length of the *jth* bundle, respectively, with the latter being found from the full-extension MR images. Also, having the current length of the segment, l_{ij}, as the distance of two adjacent nodes, its strain was obtained using Eq. (3):

$$\varepsilon_{ij}=\frac{l_{ij}\left(1+\varepsilon_j^0\right)}{l_j^r/9}-1 \tag{3}$$

in which ε_j^0 is the pre-strain of the *jth* ligament bundle. Hence, the mechanical behavior of each ligament bundle in the PFJ model was characterized using the bundle's stiffness, k_j, and pre-strain, ε_j^0, constants in Eqs. (2) and (3), respectively.

Moreover, our previous model [2] was extended to account also for the passive tensions of the muscles. For each of the three bundles of each of the six components of the quadriceps, the passive tension was found using a Hill-type model, as in Eq. (4) [41]:

$$F_{lm} = \frac{\left(K\frac{PCSA_m}{3}\right)\cdot \epsilon_{lm}}{\left(1-\frac{\epsilon_{lm}}{asym}\right)} \quad l = 1,2,3 \text{ and } m = 1,2,\ldots,6 \tag{4}$$

where $F_{lm}(N)$, and ϵ_{lm} represent the passive tension and the strain of the *lth* bundle of the *mth* component of the quadriceps, respectively. Also, $PCSA_m$ is the physiological cross-sectional area of the *mth* component of the quadriceps muscles obtained from the literature [42]. Moreover, K (N/cm^2) and *asym* are the specific strain stiffness and the strain asymptote constants of muscles, respectively, considered as 1.2 N/cm^2 and 0.7, based on the data reported for rectus femoris [41,43]. The strain of each bundle was obtained using Eq. (5):

$$\epsilon_{lm} = \frac{L_{lm}\left(1+\epsilon_m^0\right)}{L_{lm}^r} - 1 \tag{5}$$

in which L_{lm}(mm) and L_{lm}^r(mm) are the current and reference lengths of the *lth* bundle of the *mth* component of the quadriceps, respectively, and ϵ_m^0 is the pre-strain of *mth* muscle. The reference and instantaneous lengths of each quadriceps bundle were determined as the distance between its attachment points to the patella and femur, at knee full extension and each simulation step, respectively. The muscle bundles were assumed to be lax, with a pre-strain of $\epsilon_m^0 = -0.05$, considering the reports of the literature for a passively fully extended knee [17].

Using these equations, along with those of the cartilage column contact and deformation, the patellar dynamic equations of motion, etc. (see Ref. [2] for details), the model could be solved to reveal the 3D patellar tracking with respect to a fixed femur, under passive or active quadriceps loading at any knee flexion angle. The input of the model was the spatial coordinates of the tibial tubercle, i.e. the distal attachment site of the patellar tendon, which was found for the relevant knee configuration from the experiments. In simulating the PFJ laxity tests, the direction and magnitude of the perturbation force were also considered as inputs.

2.3. Ligament characterization

The aim of the characterization procedure was to identify the mechanical properties, i.e. the stiffnesses (k_j) and pre-strains (ε_j^0), of the MPFL and LPFL bundles, using the results of the calibration laxity tests. Considering the three bundles assumed for each ligament, the characterization problem included 12 unknown parameters in total (one stiffness and one pre-strain for each bundle). Having this large number of characterization parameters, it was necessary to implement a multiple-step optimization strategy to ensure finding their global optimal values within the acceptable ranges. In the first step, an identical stiffness was considered for the bundles of each of the MPFL and LPFL, reducing the number of parameters into eight. Assuming the pre-strain and stiffness to be bounded between −0.2 and 0.2, and one and nine newtons per millimeter, respectively, a total of 154 parameter sets were considered to obtain the relevant design of experiments (DOE) response surface. For each test point of the calibration laxity tests (Table 1), the PFJ model predicted the patellar motion based on a parameter set, which was then compared with the experimental data. The deviation between the model predictions and experimental results was indicated as the normalized RMS errors of the translation and rotation, to form a cost function, as in Eq. (6):

$$F(X) = \sum_{i=1}^{n}\sqrt{\frac{\sum_{j=1}^{3}\left(r_j\left(X_{ij}^{Mod}-X_{ij}^{Exp}\right)\right)^2 + \sum_{k=1}^{3}\left(r_k\left(\theta_{ik}^{Mod}-\theta_{ik}^{Exp}\right)\right)^2}{n}} \tag{6}$$

where X_{ij}^{Mod} and θ_{ik}^{Mod} are the model predictions and X_{ij}^{Exp} and θ_{ik}^{Exp} are the experiment results for the *jth* translational (in millimeters) and *kth* rotational (in radians) components of the patellar motion, respectively, for the *ith* parameter set. Also, r represents the normalization factor assumed equal to one per radian (57.3) for the rotational, and one for the translational components of the cost function. The optimal values of the stiffness and pre-strain of the MPFL and LPFL bundles were then determined using the response optimizer procedure.

In the second step of the optimization procedure, the initial values of the characterization parameters were chosen as the final values of the first step, and the ranges of variation were reduced to 1.6 to 6.3 N/mm, and −0.1 to 0.1, respectively, for the stiffness and pre-strain. This allowed us to increase the number of characterization parameters to 12, removing the pre-assumption of an identical stiffness for the three bundles of each ligament. The simulated annealing method [44,45] was then utilized to find the global minima, after 500 iterations with less than one percent change in the cost function's value.

2.4. Simulations

A number of simulations were performed using the SSJM of the PFJ, with uncharacterized and characterized ligaments, to evaluate the effect of characterization on the model's predictions. First, the calibration and validation laxity tests were simulated using the SSJM model, with the ligament properties from the literature [2], as well as those from the first and second optimization steps. Then, the passive knee flexion was simulated by the model to examine the effect of ligament characterization on the patellar motion, in comparison with the experimental data. Finally, the terminal swing instant of the gait cycle was simulated by the model, with characterized and uncharacterized ligaments. In this simulation, the knee was assumed to be fully extended and the total active force of the quadriceps muscles to be 100 N, according to the literature [46]. In addition to the initial normal condition, excessive external tibial rotations were simulated, by displacing the tibial tubercle towards lateral, in order to assess the effect of ligament characterization in an abnormal knee prone to patellar dislocation.

2.5. Sensitivity analyses

Sensitivity analyses were performed to assess the reliability of the proposed laxity test-based methodology for mechanical characterization of the PFJ ligaments. The sensitivity of the characterization procedure to the inter-individual variability of the non-characterized mechanical properties of the model components was analyzed by studying their effects on the cost function of Eq. (6). For the SSJM with the characterized MPFL and LPFL, the stiffnesses of the articular cartilage and the patellar tendon, as well as the specific strain stiffness constant of the quadriceps muscles were changed to $\pm 50\%$ of their original literature-based values, one at each step. Similarly, the pre-strain of the quadriceps components was changed to $\pm 100\%$ of its initial value. At each step, the calibration laxity tests were simulated by the model and the resulting cost function was calculated.

Furthermore, the significance of the mechanical characterization of the SSJM was studied by comparing the sensitivity of the PFJ motion to the mechanical properties of the MPFL and LPFL with those of the non-characterized model components. The stiffnesses and pre-strains of the MPFL and LPFL bundles were changed to $\pm 50\%$ and $\pm 100\%$ of their original optimal values obtained from the second characterization step (Table 2), respectively. The resulting variations in the model predictions for the patellar shift and tilt were then compared with those of the matching changes in the stiffnesses of the articular cartilage and the patellar tendon, as well as the specific strain stiffness constant and the pre-strain of the quadriceps muscles.

3. Results

The displacement–force results of the PFJ laxity tests are illustrated in Figure 6. For all curves, the zero point represents the neutral position of the patella (no perturbing force) and the slope indicates the compliance (inverse of the stiffness) of the patellar movement. In general, the patellar movement had a smaller compliance at higher flexion angles (tests 2 and 3 vs. 1 and 4, respectively), and under laterally oriented perturbing forces (tests 1 and 2 vs. 3 and 4), as expected. The displacement–force curves were highly repeatable with an overall test–retest correlation coefficient of 0.996.

The results of the first and second steps of the optimization procedure are illustrated in Figures 7 and 8, and Table 2. In general, the stiffness and pre-strain had a similar order of influence on the RMS of the deviations between the model and experimental results, and consequently the cost function value (Figure 7). The optimization procedure showed a convergence trend for the optimal parameters and reduced the value of the cost function from 6.1 to 3.9 and then to 3.0 (Table 2). As illustrated in Figure 8, ligament characterization affected mostly the model predictions for the patellar shift, tilt and rotation, with least effect on the patellar flexion, and distal–proximal and anterior–posterior translations. The optimal mechanical properties found for the ligaments indicated stiffnesses within the ranges of 2.6 and 3.8 N/mm for the LPFL, and 1.9 and 2.6 N/mm for the MPFL bundles. Also, the bundles of both ligaments were found to be relaxed in the reference (unloaded full extension) configuration, except for the most proximal bundle of the MPFL that experienced a 0.05 pre-strain.

The predictions of the PFJ model improved considerably after ligament characterization. For the validation laxity test (which was not used in the characterization procedure), the RMS of the deviations with the experimental results reduced from 6.2 mm to 0.5 mm for the patellar shift, and from 8.4° to 1.5° for the patellar tilt (Figure 9). Similarly, for the passive knee flexion test, ligament characterization decreased the deviations between model predictions and experimental results from 1.4 mm to

Table 2
Mechanical parameters of the patellofemoral ligaments before and after characterization.

Ligament properties	ε_{MPFL}			ε_{LPFL}			K_{MPFL} (N/mm)			K_{LPFL} (N/mm)			Cost function
	Bundle 1	Bundle 2	Bundle 3	Bundle 1	Bundle 2	Bundle 3	Bundle 1	Bundle 2	Bundle 3	Bundle 1	Bundle 2	Bundle 3	
Literature [2]	0.1	0.1	0.1	0.05	0.05	0.05	3.3	3.3	3.3	3.3	3.3	3.3	6.1
Step 1: characterization	0.04	0.03	0.0	−0.02	−0.02	0.0	3.3	3.3	3.3	4.2	4.2	4.2	3.9
Step 2: characterization	0.05	−0.02	−0.02	−0.01	−0.07	−0.09	2.6	1.9	1.9	3.8	3.2	2.6	3.0

LPFL, lateral patellofemoral ligament; MPFL, medial patellofemoral ligament.

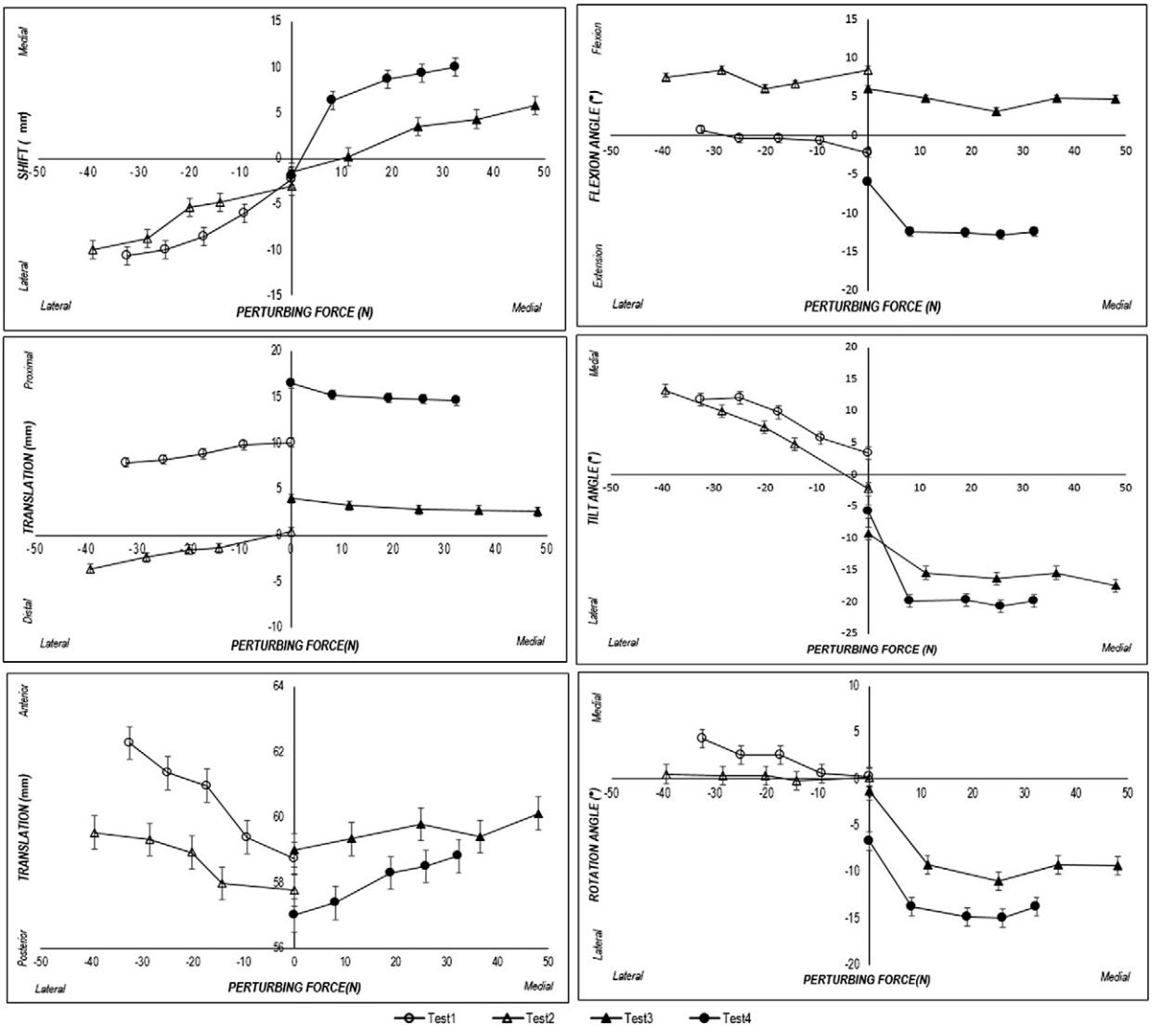

Figure 6. Displacement–force results of the patellofemoral joint laxity tests (Table 1). The patellar translations and rotations are described based on the coordinate systems defined in Figure 5.

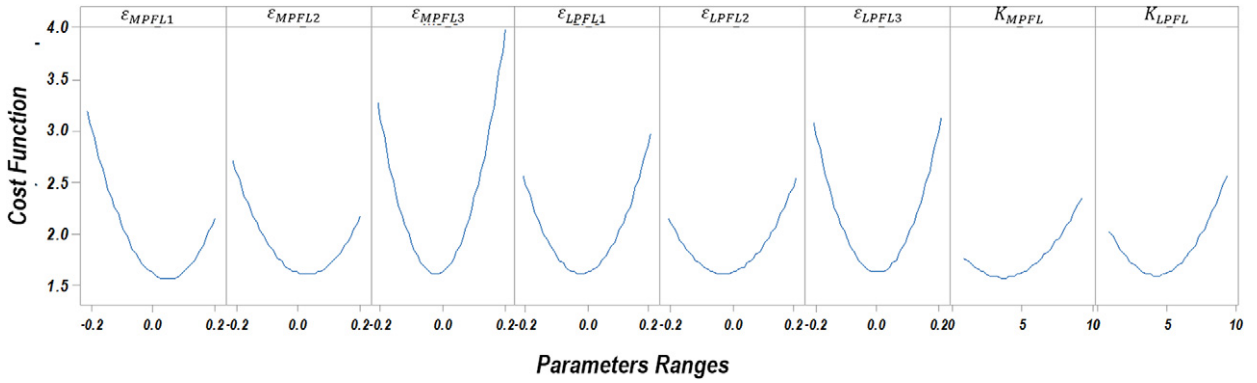

Figure 7. The main effects plot of the first step of the optimization procedure showing the effect of stiffness (K) of MPFL and LPFL, and pre-strain (ε) of each of their bundles on the cost function of Eq. (3).

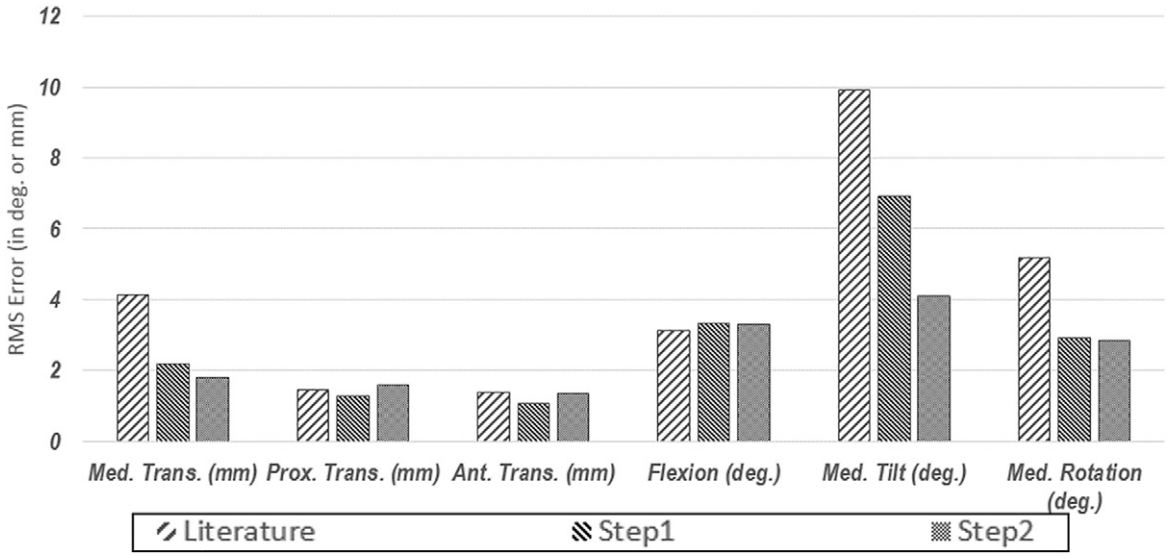

Figure 8. The overall root mean square deviations between the model predictions (based on the ligament properties from the literature and the first and second optimization steps) and the experimental results for the calibration laxity tests (Table 1).

0.3 mm and from 2.3° to 1.3° for the patellar shift and tilt, respectively (Figure 10). A substantial effect was also observed for ligament characterization when simulating abnormal knees with excessive external tibial rotations at the terminal swing instant of the gait cycle (Figure 11); the characterized model predicted four millimeters larger shift and six degrees larger tilt than the uncharacterized model in a knee with 20° excessive rotation.

The results of the sensitivity analyses are illustrated in Table 3 and Figure 12. For the SSJM with the characterized MPFL and LPFL, the effect of alteration of the non-characterized mechanical properties of model components, by ±50% for the stiffness and ±100% for the pre-strain, on the cost function of the characterization procedure (Eq. (6)) was reasonably small; the cost function remained in the range of 2.7–3.6 (Table 3). Also, simulation of three test points of each calibration laxity test by the PFJ model with altered mechanical properties of components revealed that the mechanical characteristics of the MPFL and LPFL had substantially larger effects on the patellar shift and tilt, in compassion with those of the non-characterized model components (Figure 12). The variations of the patellar shift and tilt, caused by changing the mechanical properties of the MPFL and LPFL, were in the range of 0.9–2.7 mm and 0.9–4.3° on average, respectively, significantly larger ($P < 0.05$) than those resulted from changing the other mechanical properties, i.e. 0.1–0.3 mm and 0.3–1.0°.

4. Discussion

This study is a first step towards truly subject-specific modeling of the PFJ of living individuals, to be used for personalized preplanning of the clinical interventions in patients suffering from joint disorders. In the proposed methodology, the mechanical properties of the MPFL and LPFL, as the major passive soft structures of the PFJ, are characterized using well-controlled in vivo laxity tests and a model based inverse characterization procedure. To the best of our knowledge, this study is the first in the

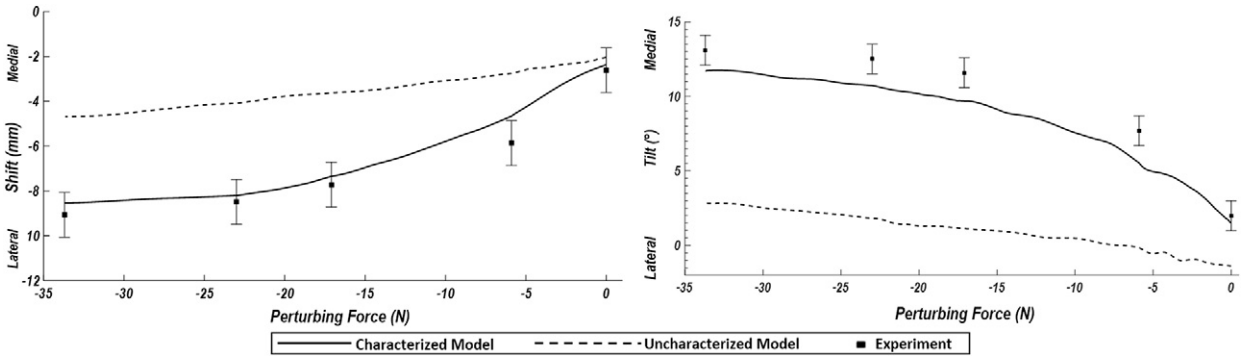

Figure 9. The predictions of the model, before and after characterization, for the patellar shift and tilt during validation laxity test, in comparison with the experimental results.

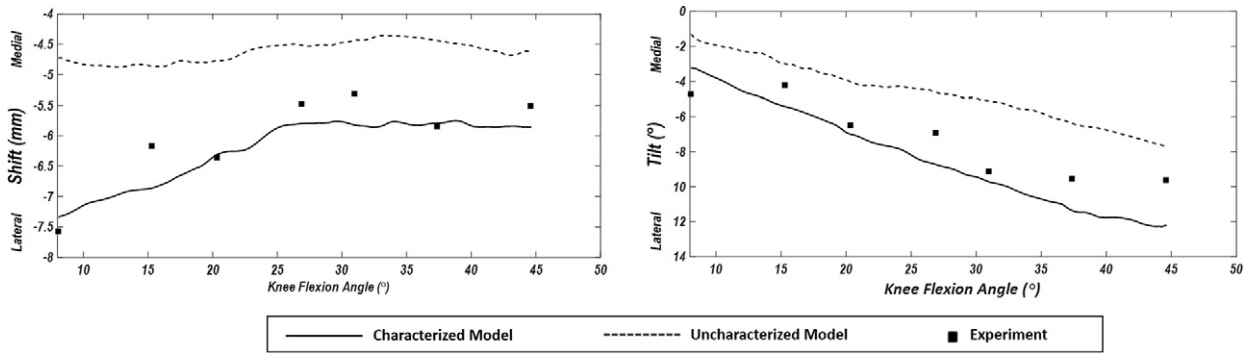

Figure 10. The predictions of the model, before and after characterization, for the patellar shift and tilt during passive knee flexion test, in comparison with the experimental results.

literature that utilizes in vivo characterization tests for subject-specific modeling of the PFJ, although a similar approach has been employed previously for modeling of the cadaver joints using in vitro experiments [4,5,47–50].

In order to assess the effectiveness of the proposed methodology, it was implemented on a normal subject and the changes of the model predictions before and after ligament characterization were studied. Considering the single subject limitation, the results of this study cannot be generalized. However, the overall findings indicate that the proposed procedure for 3D in vivo laxity testing of the PFJ is applicable and provides repeatable results. They also indicate that the multi-step optimization procedure employed is effective and demonstrates a convergence trend towards global minima with reasonable optimal results. Finally, they suggest that the proposed methodology for mechanical characterization of the PFJ ligaments is practical and can considerably improve the model predictions for the patellar shift and tilt, as the main parameters affecting the joint stability behavior. The latter finding is supported by the results of the sensitivity analysis (Figure 12) which indicate that the mechanical characteristics of the MPFL and LPFL have significantly larger effects on the patellar shift and tilt, in compassion with those of the non-characterized model components, i.e. the stiffnesses of the articular cartilage and the patellar tendon, and the specific strain stiffness constant and the pre-strain of the quadriceps muscles.

Our results for the optimized mechanical properties of the ligaments of the subject under investigation (Table 2) are within the variability range reported in previous cadaveric studies. For instance, Conlan et al. [51] reported a range of five to 16 N/mm for the stiffness of MPFL, which is comparable with the 6.4 N/mm total stiffness found in our study for the three MPFL bundles (6.4 N/mm). Similarly, the 9.6 N/mm total stiffness we found for the LPFL bundles is within the eight- to 32-N/mm range reported by Merican et al. [28] for this ligament. Nevertheless, there are also reports of higher stiffness ranges in the literature [52,53], presumably due to the ligaments' nonlinear mechanical behavior. While the cadaveric studies often report the slope of the linear region of the force–deformation curve as the ligament stiffness, at the relatively small perturbing force of our study, the ligaments are deformed in the 'toe' region of this curve, similar to during physiological activities [40,41].

The results of our study suggest that ligament characterization affects the model predictions considerably. This effect was most substantial when the patella experienced large mediolateral movements, e.g., during the validation laxity test (Figure 9) and at the terminal swing instant for a knee with excessive external tibial rotation (Figure 10). Although the latter data was not validated experimentally, this behavior is not surprising considering the fact that with large patellar mediolateral movements, the passive elastic stabilizers of the PFJ, i.e. MPFL and LPFL, will experience large tensions and their restraining effects become very significant. Nevertheless, even for the passive knee flexion test of our normal subject (Figure 10), the model predictions improved considerably after ligament characterization.

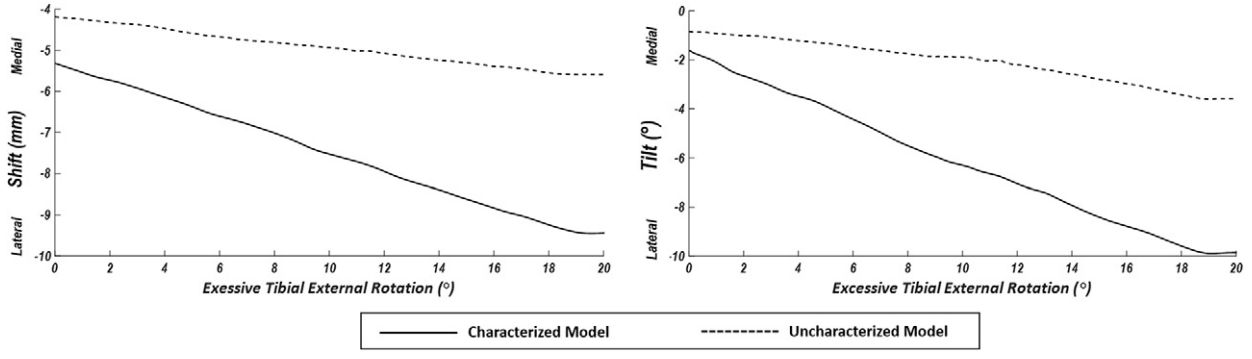

Figure 11. The predictions of the model, before and after characterization, for the patellar shift and tilt at the terminal swing instant of the gait cycle. The results are shown for excessive external tibial rotations from zero (normal knee) to 20°.

Table 3
Effects of changing the non-characterized mechanical properties on the characterization cost function.

Mechanical properties of model components	Change	Cost function
From literature [2] (ligaments uncharacterized)	–	6.1
From literature [2] (ligaments characterized)	–	3.0
Stiffness of articular cartilage (ligaments characterized)	+50%	3.1
	−50%	3.0
Stiffness of patellar tendon (ligaments characterized)	+50%	3.1
	−50%	3.1
Specific strain stiffness constant of muscles (ligaments characterized)	+50%	2.7
	−50%	3.5
Pre-strain of quadriceps components (ligaments characterized)	+100%	2.8
	−100%	3.6

There are some shortcomings concerning the data and assumptions of our PFJ model that need to be addressed. The model only included the MPFL, the LPFL and the patellar tendon, as the joint's passive structures, neglecting the effects associated with other soft tissues, such as patellotibial and patellominiscal ligaments, retinacula, and joint capsule. This limitation was mainly due to the fact that there is no adequate data available in the literature for the geometry and mechanical properties of these tissues, and their identification would increase the number of unknowns and cause complications in the optimization procedure. Also, the MPFL and LPFL were modeled as non-linear elastic materials and their viscoelastic behavior was neglected for the same reason. Moreover, the mechanical properties of the non-characterized model components, i.e. the stiffnesses of the articular cartilage and the patellar tendon, and the specific strain stiffness constant and the pre-strain of the quadriceps muscles were based on the literature and were not subject specific. The results of the sensitivity analysis, however, indicate that the effect of these parameters on the characterization cost function is minimal. Furthermore, despite efforts made to identify the attachment points of the muscles and ligaments into the bones, this procedure involved uncertainties that could have affected the results. Such simplifications might be responsible, at least in part, for the deviation of the model predictions from the experimental results, even after ligament characterization (Figures 9 and 10). Improved results might be obtained using a more sophisticated PFJ model, with more detailed and accurate representation of the anatomical structures and enhanced quadriceps simulation.

Nevertheless, the effectiveness of the characterization strategy, implemented in our study, is also a matter of concern. Obviously, a characterization problem with a large number of unknown parameters is prone to be trapped in local minima. We used a two-step optimization scheme, including DOE response surface modeling, to limit the parameters' ranges of variations, and simulated annealing, to find the final global optimums. In fact, there is a convergence trend in the course of change of the optimal parameters found in our first and second optimization steps (Table 2), that supports global optimization. However, the uniqueness of the identified parameters is still under question; there might be several different parameter sets that produce equally small cost functions. The question of uniqueness in such identification problems is often tackled by increasing the quantity

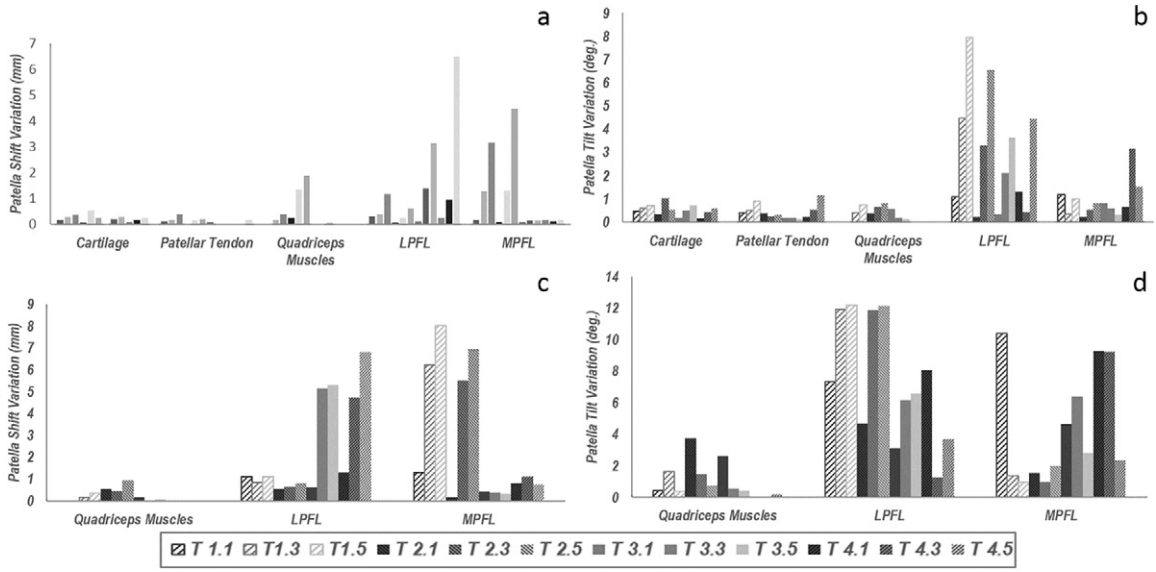

Figure 12. The variations of the model predictions for patellar shift and tilt due to (a,b) changing the stiffnesses of the articular cartilage, patellar tendon, quadriceps muscles, LPFL and MPFL by ±50% (a, b), and changing the pre-strains of the quadriceps muscles, LPFL and MPFL by ±100% (c,d), when simulating the three test points of each calibration laxity test.

of the experimental data [54]. The arrangement of our biplane fluoroscopy system, however, limited the direction and magnitude of the external load that could be applied to the patella during the laxity tests. With a more flexible setup, the patellar kinematics can be measured in other configurations of laxity test, providing a larger number of experimental data points.

As a general conclusion, the proposed methodology is promising for in vivo characterization of the ligaments in the subject-specific models of the PFJ. With further improvements in the laxity test setup and protocols, it can be used for developing clinically useful SSJMs for patients with PFJ disorders, with the capability of predicting the outcomes of prospective surgical treatments. Performing the 3D laxity tests, however, is technically demanding and costly. The currently available biplane fluoroscopy systems are mostly those developed for cardiovascular and neurovascular interventional procedures. The radiation dose of such systems is quite safe for a half an hour operation period which is required for laxity tests, thanks to the advances in digital image technology. However, they are very expensive and not usually available in medical imaging centers. With their increasing applications in orthopedic diagnostic tests, e.g., for 3D tracking of joints, it is expected that specially designed biplane fluoroscopy systems for orthopedics will be introduced in the future that can make the proposed methodology affordable for routine clinical practice.

Acknowledgments

The authors wish to thank the staff of the imaging center of IK hospital, Tehran, Iran for their help in performing the experimental part of this work. This study was supported by a research grant from Deputy of Research of Sharif University of Technology.

Conflicts of interest

The authors have no conflicts of interest to declare.

References

[1] Adouni M, Shirazi-Adl A, Shirazi R. Computational biodynamics of human knee joint in gait: from muscle forces to cartilage stresses. J Biomech 2012;45:2149–56. https://doi.org/10.1016/j.jbiomech.2012.05.040.
[2] Akbar M, Farahmand F, Jafari A, Foumani MS. A detailed and validated three dimensional dynamic model of the patellofemoral joint. J Biomech Eng 2012; 134:041005. https://doi.org/10.1115/1.4006403.
[3] Akbarshahi M, Fernandez JW, Schache AG, Pandy MG. Subject-specific evaluation of patellofemoral joint biomechanics during functional activity. Med Eng Phys 2014;36:1122–33. https://doi.org/10.1016/j.medengphy.2014.06.009.
[4] Baldwin MA, Clary C, Maletsky LP, Rullkoetter PJ. Verification of predicted specimen-specific natural and implanted patellofemoral kinematics during simulated deep knee bend. J Biomech 2009;42:2341–8. https://doi.org/10.1016/j.jbiomech.2009.06.028.
[5] Baldwin MA, Clary CW, Fitzpatrick CK, Deacy JS, Maletsky LP, Rullkoetter PJ. Dynamic finite element knee simulation for evaluation of knee replacement mechanics. J Biomech 2012;45:474–83. https://doi.org/10.1016/j.jbiomech.2011.11.052.
[6] Besier TF, Gold GE, Beaupré GS, Delp SL. A modeling framework to estimate patellofemoral joint cartilage stress in vivo. Med Sci Sports Exerc 2005;37:1924–30.
[7] Caruntu DI, Hefzy MS. 3-D anatomically based dynamic modeling of the human knee to include tibio-femoral and patello-femoral joints. J Biomech Eng 2004;126: 44–53.
[8] Elias JJ, Bratton DR, Weinstein DM, Cosgarea AJ. Comparing two estimations of the quadriceps force distribution for use during patellofemoral simulation. J Biomech 2006;39:865–72. https://doi.org/10.1016/j.jbiomech.2005.01.030.
[9] Mesfar W, Shirazi-Adl A. Knee joint mechanics under quadriceps-hamstrings muscle forces are influenced by tibial restraint. Clin Biomech 2006;21:841–8. https://doi.org/10.1016/j.clinbiomech.2006.04.014.
[10] Mesfar W, Shirazi-Adl A. Knee joint biomechanics in open-kinetic-chain flexion exercises. Clin Biomech 2008;23:477–82. https://doi.org/10.1016/j.clinbiomech.2007.11.016.
[11] Cohen ZA, Henry JH, McCarthy DM, Mow VC, Ateshian GA. Computer simulations of patellofemoral joint surgery patient-specific models for tuberosity transfer. Am J Sports Med 2003;31:87–98.
[12] Neptune R, Wright I, van den Bogert AJ. The influence of orthotic devices and vastus medialis strength and timing on patellofemoral loads during running. Clin Biomech 2000;15:611–8.
[13] Oka S, Matsushita T, Kubo S, Matsumoto T, Tajimi H, Kurosaka M, et al. Simulation of the optimal femoral insertion site in medial patellofemoral ligament reconstruction. Knee Surg Sports Traumatol Arthrosc 2014;22:2364–71. https://doi.org/10.1007/s00167-014-3192-1.
[14] Iravani M, Farahmand F, Medhipour S, Hovittalab M. Pre-planning of high tibial osteotomy: the effect of ligamentous tissues. Bone Joint J Orthop Proc Suppl 2016; 98-B:28.
[15] Senavongse W, Amis A. The effects of articular, retinacular, or muscular deficiencies on patellofemoral joint stability. Bone Joint J 2005;87:577–82.
[16] Farahmand F, Tahmasbi MN, Amis A. The contribution of the medial retinaculum and quadriceps muscles to patellar lateral stability — an in-vitro study. Knee 2004;11:89–94.
[17] Farahmand F, Tahmasbi MN, Amis AA. Lateral force–displacement behaviour of the human patella and its variation with knee flexion — a biomechanical study in vitro. J Biomech 1998;31:1147–52. https://doi.org/10.1016/s0021-9290(98)00125-0.
[18] Nikku R, Nietosvaara Y, Aalto K, Kallio PE. The mechanism of primary patellar dislocation: trauma history of 126 patients. Acta Orthop 2009;80:432–4. https://doi.org/10.3109/17453670903110634.
[19] Fulkerson JP. Disorders of the patellofemoral joint. Baltimore: Williams and Wilkins; 1997.
[20] Fulkerson JP. Diagnosis and treatment of patients with patellofemoral pain. Am J Sports Med 2002;30:447–56.
[21] Nomura E, Inoue M. Surgical technique and rationale for medial patellofemoral ligament reconstruction for recurrent patellar dislocation. Art Ther 2003;19:E47. https://doi.org/10.1053/jars.2003.50167.
[22] Zhang L, Li ZY, Liu JS, Sun J, Ma J, Zhang S. Injury and reconstruction of medial patellofemoral ligament. Zhongguo Gu Shang 2010;23:189–93.
[23] Nomura E, Horiuchi Y, Kihara M. Medial patellofemoral ligament restraint in lateral patellar translation and reconstruction. Knee 2000;7:121–7. https://doi.org/10.1016/s0968-0160(00)00038-7.
[24] Müller JH, Scheffer C, Elvin A, Erasmus PJ, Drillon EM. Patella tracking with peripatellar soft tissues stabilizers as a function of dynamic subject-specific knee flexion. J Mech Med Biol 2011;11:1025–43. https://doi.org/10.1142/S0219519411004332.
[25] Kang HJ, Wang F, Chen BC, Su YL, Zhang ZC, Yan CB. Functional bundles of the medial patellofemoral ligament. Knee Surg Sports Traumatol Arthrosc 2010;18: 1511–6.
[26] Nomura E, Inoue M, Osada N. Anatomical analysis of the medial patellofemoral ligament of the knee, especially the femoral attachment. Knee Surg Sports Traumatol Arthrosc 2005;13:510–5.
[27] Merican AM, Amis AA. Anatom of the lateral retinaculum of the knee. Bone Joint J 2008;90-B:527–34. https://doi.org/10.1302/0301-620x.90b4.20085.

[28] Merican AM, Sanghavi S, Iranpour F, Amis AA. The structural properties of the lateral retinaculum and capsular complex of the knee. J Biomech 2009;42:2323–9.
[29] Amis AA, Firer P, Mountney J, Senavongse W, Thomas NP. Anatomy and biomechanics of the medial patellofemoral ligament. Knee 2003;10:215–20.
[30] Kaptein BL, Shelburne KB, Torry MR, Giphart JE. A comparison of calibration methods for stereo fluoroscopic imaging systems. J Biomech 2011;44:2511–5.
[31] Bey MJ, Kline SK, Tashman S, Zauel R. Accuracy of biplane x-ray imaging combined with model-based tracking for measuring in-vivo patellofemoral joint motion. J Orthop Surg Res 2008;3. https://doi.org/10.1186/1749-799X-3-38.
[32] Giphart JE, Zirker CA, Myers CA, Pennington WW, LaPrade RF. Accuracy of a contour-based biplane fluoroscopy technique for tracking knee joint kinematics of different speeds. J Biomech 2012;45:2935–8. https://doi.org/10.1016/j.jbiomech.2012.08.045.
[33] Suzuki T, Hosseini A, Li JS, Gill TJt, Li G. In vivo patellar tracking and patellofemoral cartilage contacts during dynamic stair ascending. J Biomech 2012;45:2432–7. https://doi.org/10.1016/j.jbiomech.2012.06.034.
[34] Eskandari A, Arjmand N, Shirazi-Adl A, Farahmand F. Subject-specific 2D/3D image registration and kinematics-driven musculoskeletal model of the spine. J Biomech 2017;57:18–26.
[35] Guoan L, Sakamoto M, Chao EYS. A comparison of different methods in predicting static pressure distribution in articulating joints. J Biomech 1997;30:635–8.
[36] Jafari A, Farahmand F, Meghdari A. The effects of trochlear groove geometry on patellofemoral joint stability — a computer model study. Proc Inst Mech Eng H 2008;222:75–88.
[37] Blankevoort L, Huiskes R. Validation of a three-dimensional model of the knee. J Biomech 1996;29:955–61.
[38] Blankevoort L, Kuiper JH, Huiskes R, Gootenboer HJ. Articular contact in a three-dimensional model of the knee. J Biomech 1991;24:1019–31.
[39] Mesfar W, Shirazi-Adl A. Biomechanics of the knee joint in flexion under various quadriceps forces. Knee 2005;12:424–34. https://doi.org/10.1016/j.knee.2005.03.004.
[40] Fung YC. Biomechanics: mechanical properties of living tissues. New York: Springer-Verlag; 1981.
[41] Deng Y-C, Goldsmith W. Response of a human head/neck/upper-torso replica to dynamic loading — II. Analytical/numerical model. J Biomech 1987;20:487–97.
[42] Farahmand F, Sejiavongse W, Amis AA. Quantitative study of the quadriceps muscles and trochlear groove geometry related to instability of the patellofemoral joint. J Orthop Res 1998;16:136–43.
[43] Yamada H, Evans FG. Strength of biological materials. Baltimore: Williams & Wilkins; 1970.
[44] Corana A, Marchesi M, Martini C, Ridella S. Minimizing multimodal functions of continuous variables with the “simulated annealing” algorithm: corrigenda for this article is available here. ACM Trans Math Softw 1987;13:262–80.
[45] Kirkpatrick S, Gelatt CD, Vecchi MP. Optimization by simulated annealing. Science 1983;220:671–80.
[46] Besier TF, Fredericson M, Gold GE, Beaupré GS, Delp SL. Knee muscle forces during walking and running in patellofemoral pain patients and pain-free controls. J Biomech 2009;42:898–905.
[47] Ali A, Mannen E, Smoger L, Haas B, Laz P, Rullkoetter P, et al. Evaluation of in-vivo mechanics for medialised dome and medialised anatomic patellofemoral geometries during knee extension and lunge. Bone Joint J 2017;99:10.
[48] Ali AA, Harris MD, Shalhoub S, Maletsky LP, Rullkoetter PJ, Shelburne KB. Combined measurement and modeling of specimen-specific knee mechanics for healthy and ACL-deficient conditions. J Biomech 2017;57:117–24.
[49] Ali AA, Shalhoub SS, Cyr AJ, Fitzpatrick CK, Maletsky LP, Rullkoetter PJ, et al. Validation of predicted patellofemoral mechanics in a finite element model of the healthy and cruciate-deficient knee. J Biomech 2016;49:302–9. https://doi.org/10.1016/j.jbiomech.2015.12.020.
[50] Harris MD, Cyr AJ, Ali AA, Fitzpatrick CK, Rullkoetter PJ, Maletsky LP, et al. A combined experimental and computational approach to subject-specific analysis of knee joint laxity. J Biomech Eng 2016;138. https://doi.org/10.1115/1.4033882.
[51] Conlan T, Garth Jr W, Lemons JE. Evaluation of the medial soft-tissue restraints of the extensor mechanism of the knee. J Bone Joint Surg Am 1993;75:682–93.
[52] Edington C, Gonzales O, Woo SL. Characterization of the structural properties of the human medial patello-femoral ligament. In: Woo SL-Y, editor. Musculoskeletal Research Center Summer Research Program 2008. University of Pittsburgh; 2008. p. 19.
[53] Kim KE, Hsu SL, Woo SLY. Tensile properties of the medial patellofemoral ligament: the effect of specimen orientation. J Biomech 2014;47:592–5. https://doi.org/10.1016/j.jbiomech.2013.11.026.
[54] Avril S, Evans S, Miller K. Inverse problems and material identification in tissue biomechanics. J Mech Behav Biomed Mater 2013;27:129–31.